JACS
JOURNAL OF THE AMERICAN CHEMICAL SOCIETY
Article
pubs.acs.org/JACS

A New Family of Perovskite Catalysts for Oxygen-Evolution Reaction in Alkaline Media: $BaNiO_3$ and $BaNi_{0.83}O_{2.5}$

Jin Goo Lee,[†,§] Jeemin Hwang,[†,§] Ho Jung Hwang,[‡] Ok Sung Jeon,[†] Jeongseok Jang,[†] Ohchan Kwon,[†] Yeayeon Lee,[‡] Byungchan Han,[*,†] and Yong-Gun Shul[*,†]

[†]Department of Chemical and Bio-molecular Engineering, Yonsei University, 134 Shinchon-dong, Seodaemun-gu, Seoul 120-749, Republic of Korea

[‡]Department of Graduate Program in New Energy and Battery Engineering, Yonsei University, 134 Shinchon-dong, Seodaemun-gu, Seoul 120-749, Republic of Korea

Supporting Information

ABSTRACT: Establishment of a sustainable energy society has been strong driving force to develop cost-effective and highly active catalysts for energy conversion and storage devices such as metal−air batteries and electrochemical water splitting systems. This is because the oxygen evolution reaction (OER), a vital reaction for the operation, is substantially sluggish even with precious metals-based catalysts. Here, we show for the first time that a hexagonal perovskite, $BaNiO_3$, can be a highly functional catalyst for OER in alkaline media. We demonstrate that the $BaNiO_3$ performs OER activity at least an order of magnitude higher than an IrO_2 catalyst. Using integrated density functional theory calculations and experimental validations, we unveil that the underlying mechanism originates from structural transformation from $BaNiO_3$ to $BaNi_{0.83}O_{2.5}$ ($Ba_6Ni_5O_{15}$) over the OER cycling process.

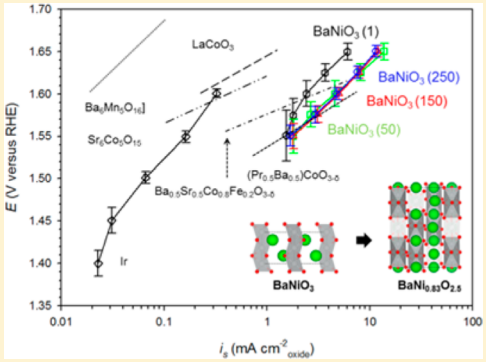

INTRODUCTION

Oxygen evolution reaction (OER) is a vital process for diverse energy storage devices. For instance, the rechargeable metal−air batteries ($M_xO_2 \rightarrow M_x + O_2$)[1,2] and fuel generation through water splitting reactions ($H_2O \rightarrow H_2 + 1/2O_2$)[3] are two archetype examples. The efficiency of the systems is critically dependent on the OER, but even with precious metal catalysts, the low activity is still a major concern leading to significant overpotential. Recently, it was proposed that perovskite oxides produced high OER activity comparable to state-of-the-art IrO_2; ever since a number of researches have been focused on the development of the perovskite structure catalysts and identification of essential descriptors of OER activity from fundamental perspective.[4−13] A perovskite oxide (crystal structure ABO_3 where A is a rare-earth or alkaline-earth metal and B is a transition metal) is more cost-effective and highly active compared with conventionally utilized noble metals and is pliable in physical, chemical, and catalytic properties.

Recently, using corner-shared pseudocubic perovskites in an alkaline solution ($4OH^- \rightarrow O_2 + 2H_2O + 4e^-$), Suntivich et al.[5] suggested that the filling of e_g level electrons of the surface cation can be a descriptor for OER activity. They proposed that the OER activity is high because the occupancy is close to one and the degree of the covalency in the chemical bond between the transition metal and oxygen is high.[5] We realized that few studies have been published on hexagonal perovskite catalysts for the OER despite numerous reports on perovskite catalysts.[6−12] Grimaud et al. reported the OER activity and stability of hexagonal perovskite oxides ($Ba_6Mn_5O_{16}$ and $Sr_6Co_5O_{15}$).[13] They suggested that the electronic structure of transition metal oxides, such as face-shared (f-s) and prism (P) in hexagonal perovskites, plays a critical role in the OER activity and stability.

We focused on a $BaNiO_3$ ($Ba_6Ni_5O_{15}$) material (t = ∼1.13, t refers to Goldschmidt's tolerance factor), which has a hexagonal perovskite structure with the face-shared (f-s) [NiO_6] octahedral oriented to chain units $(NiO_3)_\infty^{\infty-}$. The Ni oxidation states are crystallographically equivalent in $BaNiO_3$, but it has been suggested that intermediate phases, $BaNiO_x$ ($2.3 < x < 2.67$) and $BaNi_{0.83}O_{2.5}$ ($Ba_6Ni_5O_{15}$), derived from phase transformations of $BaNiO_3$ induce supermixed valence states of Ni^{2+}, Ni^{3+}, and Ni^{4+},[14−16] developing the distorted-prism (P) coordination. The mixed oxidation state can promote OER activity via redox reaction of *OOH (known as a rate-determining step in OER), which might be fast.[11,17−19]

However, the crystal and electronic structures of $BaNiO_3$ and $BaNi_{0.83}O_{2.5}$ have never been investigated under the context of electrochemistry for energy applications. Here, we provided fundamental information on hexagonal perovskites of $BaNiO_3$ and $BaNi_{0.83}O_{2.5}$ as new candidates of perovskite-type catalysts for the OER. The OER activity of the $BaNiO_3$ was improved during the OER cycles, which is far beyond of the state-of-the-

Received: January 11, 2016
Published: February 24, 2016

DOI: 10.1021/jacs.6b00036
J. Am. Chem. Soc. 2016, 138, 3541−3547

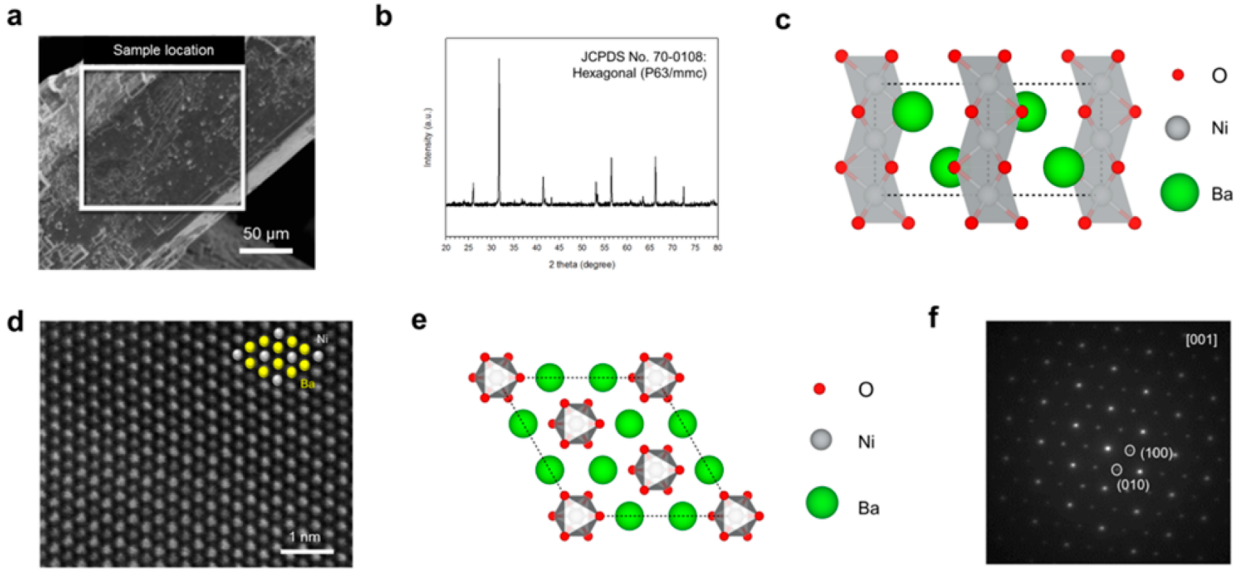

Figure 1. Morphology and crystal structures of the $BaNiO_3$. (a) SEM image of the $BaNiO_3$ synthesized via flux-mediated crystal growth. White rectangle represents the sample position for the TEM analysis. The $BaNiO_3$ was a hexagonal-rod shape with a thickness of ∼100 μm. (b) XRD patterns of the $BaNiO_3$. It corresponds to a hexagonal perovskite structure with space group $P6_3/mmc$. (c) Schematic of the $BaNiO_3$ crystal structure. The face-shared (f-s) NiO_6 octahedra form chains running along [001]. (d) Atomic-level HADDF image of the $BaNiO_3$. (e) Schematic of the $BaNiO_3$ crystal structure. It shows identical atomic arrangements with the $BaNiO_3$ as shown in the HADDF image. The interatomic distances of Ba−Ni and Ni−Ni were ∼3.523 and ∼5.802 Å, respectively. It corresponds to the results obtained from the structural modeling data. (f) SAED pattern along the [001] zone axis. The $BaNiO_3$ synthesized via flux-mediated crystal growth has a single-crystalline feature.

art IrO_2 catalyst over OER cycling experiments. Using density functional theory calculations, we unveiled the underlying mechanism leading to the high OER catalytic activity of the $BaNi_{0.83}O_{2.5}$. We setup the model systems of three perovskites of $BaNi_{0.83}O_{2.5}$, $BaNiO_2$, and $BaNiO_3$ to carefully analyze variations of the electronic as well as geometrical structures. To explicitly represent the OER activity, we calculated thermodynamic free energy diagrams for each of the three perovskite model systems. Using integrated experimental analysis and density functional theory (DFT) calculations, we found that the high activity of the $BaNiO_3$ can be derived from a natural phase transformation from $BaNiO_3$ to $BaNi_{0.83}O_{2.5}$ during the OER cycling process. Our finding suggested that the Ni-based hexagonal perovskites can be promising for OER catalysts meeting the principles previously speculated.[5,9,17]

RESULTS AND DISCUSSION

The hexagonal perovskite $BaNiO_3$ was synthesized via flux-mediated crystal growth.[20] The $BaNiO_3$ has hexagonal-rod shapes with an average thickness of 100 μm (Figure 1a and Figure S1). EDS measurements indicate that the $BaNiO_3$ crystal was composed of Ba and Ni with an atomic ratio of ∼1:1 (Table S1). Moreover, Ba and Ni atoms were uniformly distributed across the whole sheet (Figure S2), indicating the uniform chemical composition. The crystal structure of the $BaNiO_3$ was refined in hexagonal symmetry with space group $P6_3/mmc$ and unit-cell parameters $a = b = 5.660$ Å and $c = 4.801$ Å (Figure 1b and Table S2). Figure 1c represents the crystal structure of the $BaNiO_3$ projected down [110]. The face-shared (f-s) NiO_6 octahedra form chains running along [001]. Figure 1d shows a typical atomic-level HAADF−STEM image of ultrathin $BaNiO_3$ crystals. It can be found that all the atoms were closely packed into a hexagonal structure, and Ni atoms (dark gray) were located at the center surrounded by six Ba atoms (light gray) in the view along the [001] direction, which shows identical atomic arrangements with the crystal model as shown in Figure 1e. The interatomic distances of Ba−Ni and Ni−Ni were ∼3.523 and ∼5.802 Å, respectively. This corresponds to the results obtained from the structural modeling data (Figure S3). The SAED patterns of the $BaNiO_3$ synthesized via flux-mediated crystal growth demonstrate a single-crystalline feature (Figure 1f).

The OER currents of the $BaNiO_3$ and IrO_2 were obtained in 0.1 M KOH electrolyte by using a rotating-disk electrode at a rotating speed of 1600 rpm and at a scan rate of 10 mV s^{-1} (reference electrode Hg/HgO (Figure S4)). To separate the surface area effect from the intrinsic catalytic activity, the surface area-normalized kinetic current density (specific activity, i_s) of the $BaNiO_3$ as a function of potential versus RHE is represented in Figure 2a. The surface area of the $BaNiO_3$ was 0.301 m^2 g^{-1} (Figure S5). The initial specific current at 1.6 V was approximately 2.42 mA $cm^2{}_{oxide}$, which surpasses 0.32 mA $cm^2{}_{oxide}$ of the IrO_2. Furthermore, the currents after 50 cycles and 150 cycles were comparable to that of state-of-the-art $Ba_{0.5}Sr_{0.5}Co_{0.8}Fe_{0.2}O_{3-\delta}$ (BSCF82)[5] and $(Pr_{0.5}Ba_{0.5})CoO_{3-\delta}$,[12] showing approximately 4.56 and 4.99 mA $cm^2{}_{oxide}$, respectively (Figure 2a). With respect to the specific OER activity normalized by electrochemical surface area (ECSA), the $BaNiO_3$ catalyst after 250 cycles was also higher at 6.32 mA $cm^{-2}{}_{ECSA}$ compared with 4.52 mA $cm^{-2}{}_{ECSA}$ (initial) of the IrO_2 catalysts at 1.6 V (Figure S6 and S7).[2] The anodic current around 1.43 V appeared during 50 cycles, and the OER current was significantly enhanced simultaneously (Figure S8). The pseudocapacitance behavior can appear due to oxidation of Ni atoms as reported earlier.[21−24] Recently, some reports show that surface amorphization can enhance the OER activity in alkaline media.[10,25,26] In fact, the catalyst reported by Suntivich et al. was also unstable in base, and that their perovskite "catalyst" was actually a precursor for the active composition.[5,10] Thus, the significant increase in the OER activity

DOI: 10.1021/jacs.6b00036
J. Am. Chem. Soc. 2016, 138, 3541−3547

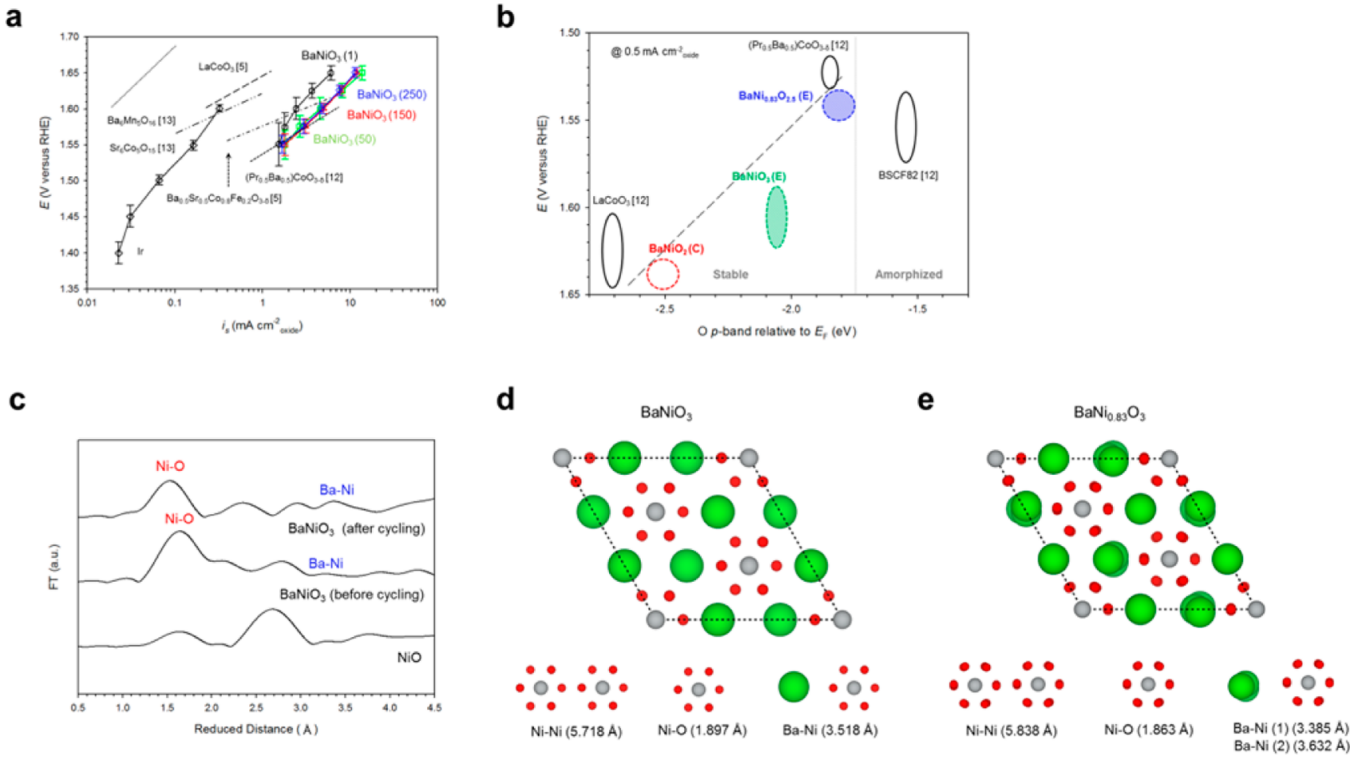

Figure 2. OER activities and phase transformation of the $BaNiO_3$. (a) OER specific activities of the $BaNiO_3$ during the OER cycles.[5,12,13] Error bars represent sd from at least five independent measurements. The specific activity after OER cycling was comparable to state-of-the-art $Ba_{0.5}Sr_{0.5}Co_{0.8}Fe_{0.2}O_{3-\delta}$ (BSCF82). (b) Evolution of the potential at 0.5 mA cm^{-2}_{oxide} versus the O p-band center relative to E_F (eV) of the $BaNiO_3$. The O p-band center relative to the Fermi level was computed by DFT. Solid outlined circles represent the results reported by other researchers, and dotted outline circles (C) represent the $BaNiO_3$, $BaNi_{0.83}O_{2.5}$, and $BaNiO_2$ calculated by DFT. The filled dotted outline circles (E) indicate the results via experimental measurements in this study. (c) Fourier transforms (FT) of EXAFS of the $BaNiO_3$ before and after the OER cycles. The Ni K-edge X-ray absorption was acquired in the TEY mode. The FT was calculated between 3.5 and 13.0 A^{-1} after weighting by k^3. Note that the interatomic distances of the Ni−O and Ba−Ni in the $BaNiO_3$ were shifted to lower and higher positions after the OER cycles, respectively. (d) Schematic of the $BaNiO_3$ crystal structure with the interatomic distances calculated by DFT. (e) Schematic of the $BaNi_{0.83}O_{2.5}$ crystal structure with the interatomic distances calculated by DFT. The shift of the interatomic distances of the $BaNiO_3$ corresponds to that of the results calculated by DFT, which demonstrates that the $BaNiO_3$ was naturally transformed into the $BaNi_{0.83}O_{2.5}$ during the OER cycles.

during 50 cycles may be attributed to the surface amorphization of the small amount of Ni species (Figure S9). Thereafter, the OER activity of the $BaNiO_3$ was stable for 1000 cycles with deactivation rate of 11.1%, which is lower than the results for IrO_2 (IrO_2 is considered to be an unstable catalyst in alkaline media[25]) and similar or slightly higher compared with the results of stable catalysts recently reported ($SrNb_{0.1}Co_{0.7}Fe_{0.2}O_{3-\delta}$, $LiCo_{0.8}Fe_{0.2}O_2$, $(La_{0.613}Ca_{0.387})_2NiO_{3.562}$, and others).[27−31] However, we believe that the OER stability can be further enhanced by several approaches such as insertion of other metal oxides or change of the composition ratio. It is well-known that the d-band center energy (ε_d) is an important descriptor for a bond strength between transition metal and an adsorbate.[32] The key idea is the higher lying is the ε_d with respect to Fermi energy the stronger is the chemisorption for the fixed d-band filling. There have been several reports that the O p-band center could work as a descriptor for OER catalysis similarly to the d-band center model,[12] that is, the closer O p-band energy center is to the Fermi energy the higher the OER activity. Our calculations showed that O p-band energy centers of $BaNiO_3$, $BaNiO_2$, and $BaNi_{0.83}O_{2.5}$ with respect to Fermi energy were −2.14, −2.49, and −1.79 eV, respectively. Therefore, OER activity of the $BaNi_{0.83}O_{2.5}$ should be the highest among the three perovskites oxides. Furthermore, The $BaNi_{0.83}O_{2.5}$ has the O p-band resembling the double perovskite, which implies that the hexagonal perovskites are stable against surface amorphization (Figure 2b and Figure S10). It can be also supported by the low deactivation rate from 150 cycles to 1000 cycles (Figure S8) and stable chronoptentiometric responces (Figure S11). Recently, Mefford et al. suggested oxygen intercalation in $LaMnO_3$ perovskite pseudocapacitor electrodes in alkaline media. The oxygen intercalation can build V^*_{Mn} (Mn vacancy) and then gives rise to manganese surface segregation.[24] In this respect, it would be possible to form Ni vacancies in the $BaNiO_3$ during the OER cycles, which leads to phase transformation into $BaNi_{0.83}O_{2.5}$ or $BaNiO_2$. To determine the phase transformation of the $BaNiO_3$, we examine the changes in the local structure obtained by analysis of the extended X-ray absorption fine structure (EXAFS) of the $BaNiO_3$ before and after OER cycling (Figure 2c). The reduced distance of Ni−O was shifted from ∼1.62 Å (interatomic distance ∼1.92 Å) to ∼1.54 Å (interatomic distance ∼1.84 Å) after the OER cycling. Moreover, the reduced distance of the Ba−Ni was also shifted from ∼3.22 Å (interatomic distance ∼3.52 Å) to 3.35 Å (interatomic distance ∼3.65 Å). These changes in the interatomic distances demonstrate the phase transformation of the $BaNiO_3$ to $BaNi_{0.83}O_{2.5}$, supported by DFT calculations (Figure 2d,e).

As another electronic structure effect, we calculated the filling of e_g-energy levels in the perovskite oxides since the e_g-orbital

DOI: 10.1021/jacs.6b00036
J. Am. Chem. Soc. 2016, 138, 3541−3547

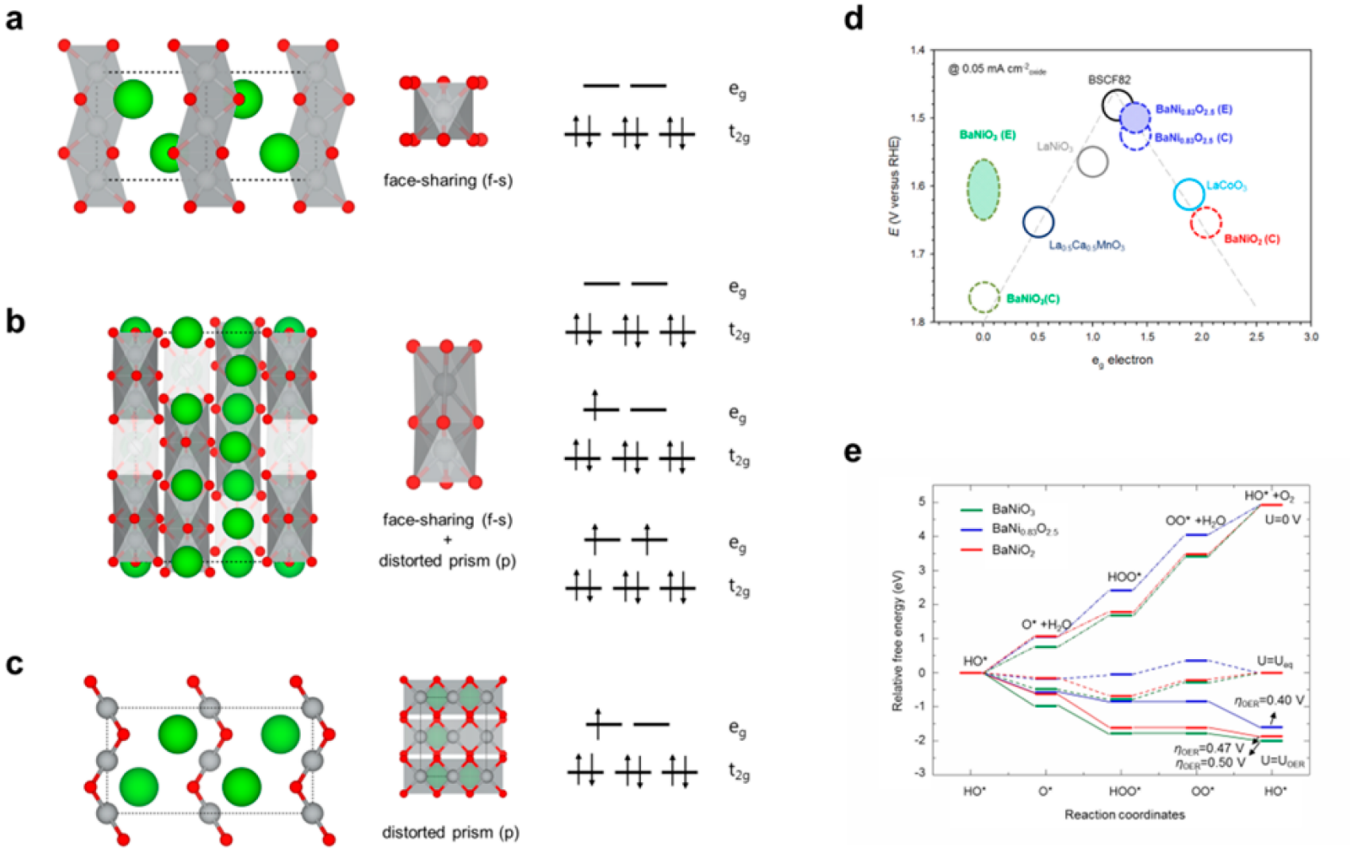

Figure 3. Schematics of phase transformation and the evidence of the OER activity of the $BaNiO_3$. (a) Schematic of the $BaNiO_3$ crystal structure with the interatomic distances calculated by DFT. (b) Schematic of the $BaNi_{0.83}O_{2.5}$ crystal structure with the interatomic distances calculated by DFT. (c) Schematic of the $BaNiO_2$ crystal structure with the interatomic distances calculated by DFT. (d) The relation between the OER catalytic activity, defined by the overpotential at 0.05 mA cm$^{-2}_{oxide}$, of OER current, and the occupancy of the e_g electron of the transition metal. Solid outline circles represent the results reported by other researchers, and dotted outline circles (C) represent the $BaNiO_3$, $BaNi_{0.83}O_{2.5}$, and $BaNiO_2$ calculated by DFT. The filled dotted outline circles (E) indicate the results via experimental measurements in this study. (e) Free energy diagrams of the $BaNiO_3$, $BaNi_{0.83}O_{2.5}$, and $BaNiO_2$ depending on the reaction coordinates.

of a d-band in the transition metal directly overlaps with the p_z orbital of oxygen leading to substantial Pauli repulsion via orbital orthogonalization. According to Sabatier's principle the e_g orbital filling should be optimized (about 1.2) to secure high OER activity as proposed by Shao-Horn's group.[5,33] We obtained the e_g-orbital fillings of 0, 2, and about 1.4 for $BaNiO_3$ (Ni^{4+} $(t_{2g})^6(e_g)^0$), $BaNiO_2$ (Ni^{2+} $(t_{2g})^6(e_g)^2$), and $BaNi_{0.83}O_{2.5}$ (Ni^{2+} $(t_{2g})^6(e_g)^1$, Ni^{3+} $(t_{2g})^6(e_g)^1$, and Ni^{4+} $(t_{2g})^6(e_g)^2$), respectively (Figure 3a–c). The schematic of the $BaNiO_2$ crystal structure is shown in Figure S12. Accordingly our results indicate that $BaNi_{0.83}O_{2.5}$ should produce the highest OER activity, and the $BaNiO_3$ should be the lowest among the three perovskite oxides. Figure 3d shows the relation between the OER catalytic activities of the $BaNiO_3$, $BaNi_{0.83}O_{2.5}$, and $BaNiO_2$ as a function of e_g electron occupancy. The OER activity of the $BaNiO_3$ was different between the results of the experimental measurements and computational DFT analysis. It may be because the phase transformation rapidly starts at the early OER cycle (Figure S13 and Table S3). In the $BaNi_{0.83}O_{2.5}$, the OER activity obtained from the experimental measurements corresponded to the computational DFT analysis. It demonstrates that the phase transformation of the $BaNiO_3$ into the $BaNi_{0.83}O_3$ leads to the enhancement of OER activity by the change in e_g electron occupancy. The high activity of the $BaNi_{0.83}O_{2.5}$ would be also attributed to the change in Ni coordination. The formation of Ni vacancies in $BaNi_{0.83}O_{2.5}$ changes the face-shared (f-s) coordination into distorted prism (P), lowering Ni oxidation states (Figure 3a,b). The Ni K-edge X-ray absorption near edge structure (XANES) spectra of the $BaNiO_3$ shows that the absorption edge position shifts toward lower energy side after the OER cycling, suggesting a concomitant decrease ($Ni^{4+} \rightarrow Ni^{2+}/Ni^{3+}$) in the Ni oxidation state (Figure S14).[34,35] X-ray absorption spectroscopy (XAS) Ni $L_{2,3}$-edge spectra provided further information on Ni oxidation states (Figure S15). It shows two characteristic lines, originated with transitions from the $2p_{3/2}$ (L_3, $2p_{3/2} \rightarrow 3d$, ~853 eV) and $2p_{1/2}$ (L_2, $2p_{3/2} \rightarrow 3d$, ~870 eV) levels (split by the spin–orbit interaction) to empty levels of the 3d band. All spectra were aligned using a NiO standard (L_3 = ~853 eV). The Ni $L_{2,3}$-edge spectra of the $BaNiO_3$ before the OER cycling showed that Ni is predominantly in a 4+ oxidation state.[36] After the OER cycling, a change in valence from Ni^{4+} to Ni^{3+}/Ni^{2+} due to oxygen nonstoichiometry of the $BaNi_{0.83}O_{2.5}$ occurs by an increase in the first peak intensity while the second peak diminished. The L_2-edge peak was also shifted from ~873 to ~870 eV. This demonstrates Ni supermixed valence in stoichiometric $BaNi_{0.83}O_{2.5}$ (Ni^{2+}, Ni^{3+}, and Ni^{4+}). XAS O 1s (K-edge) spectra reflect the O 2p weight hybridized into the unoccupied states of the transition metal and alkali rare-earth or rare-earth ions (Figure S16). The pre-edge region from ~528 to ~533 eV is described as oxygen 2p states hybridized with the transition metal 3d states. The peaks from ~534 to ~540 eV

DOI: 10.1021/jacs.6b00036
J. Am. Chem. Soc. 2016, 138, 3541–3547

can be assigned to O 2p states mixed with Ba 5d and Ni 4sp states.[37] The peak of the $BaNiO_3$ before the OER cycling appeared at ~529 eV. This feature may be associated with the presence of higher Ni oxidation state (Ni^{4+}) than Ni^{3+}.[38] After OER cycling, the peak at ~529 eV disappeared, and a new peak appeared at ~532 eV where the addition of an electron in the e_g sub-band is related. The broad peak at ~532 eV was slightly shifted from the peak of NiO at ~531.5 eV, which may be associated with the distortion of Ni coordination (e.g., e_g sub-band splitting to z^2 and $x^2 - y^2$).[38] All XAS spectra support that the Ni supermixed valence and coordination distortion are developed in the $BaNi_{0.83}O_{2.5}$. In correlation with the OER activities, this finding suggests that HS Ni^{2+} in P coordination is more active than Ni^{4+} in f-s coordination, which resembles the suggestions of Grimaud et al. on the relationship between Co coordination and OER activity.[13]

To quantitatively predict OER performance, we calculated the free energy diagram in an alkaline medium on the thermodynamic aspect. The methodology has been widely applied to various catalytic processes.[39,40] We assumed the overall OER mechanism, $4OH^- \rightarrow O_2 + 2H_2O + 4e^-$, composed with four elementary reaction steps as eqs 1−4 as suggested by Goodenough and associates.[41] We only considered intermediates involving electrons in the reactions.

$$HO^* + OH^- \rightarrow O^* + H_2O + e^- \quad (1)$$

$$\Delta G_1 = \Delta G(HO^*) - \Delta G(O^*) - \Delta G(H_2O) - (e^- - OH^-) - eU$$

$$O^* + OH^- \rightarrow HOO^* + e^- \quad (2)$$

$$\Delta G_2 = \Delta G(O^*) - \Delta G(HOO^*) - (e^- - OH^-) - eU$$

$$HOO^* + OH^- \rightarrow OO^* + H_2O + e^- \quad (3)$$

$$\Delta G_3 = \Delta G(HOO^*) - \Delta G(OO^*) - \Delta G(H_2O) - (e^- - OH^-) - eU$$

$$OO^* + OH^- \rightarrow HO^* + O_2 + e^- \quad (4)$$

$$\Delta G_4 = \Delta G(OO^*) - \Delta G(HO^*) - \Delta G(O_2) - (e^- - OH^-) - eU$$

Here, ΔG_{1-4} represent the free energy of each intermediate in the OER mechanism obtained by $\Delta G = \Delta E + \Delta ZPE - T\Delta S + eU$. ΔE is the calculated DFT energy. ΔZPE and ΔS are the change of zero point energy and entropy, respectively. These corrections are adopted from standard tables for gas phase molecules.[42] The asterisk behind an intermediate signifies the active site on the surface of perovskite. To estimate the effect of the electron's chemical potential under applied potential (U), we linearly shifted the free energy by eU. The free energy of H_2O, O_2, and OH^- was obtained by using DFT energy of H_2O and H_2 in the gas phase. The energy of H_2O is corrected with zero point energy and calculated at the pressure of 0.035 bar since the free energy of H_2O in liquid phase is the same as that in gas phase. To minimize DFT energy for oxygen, we utilized the free energy of the formation of water ($1/2O_2 + H_2 \rightarrow H_2O$), and the free energy of $OH^-(aq)$ was estimated by the reaction of $H_2O(l) = H^+(aq) + OH^-(aq)$. The free energy of OH^- was found using the overall reaction of OER ($4OH^- \rightarrow O_2 + 2H_2O + 4e^-$) in alkaline electrolyte. The overall equation can be rearranged as $\Delta G(OH^-) = \{\Delta G(total) - \Delta G(O_2) - 2\Delta G(H_2O)\}/4$. The corrected free energy of O_2 and $2H_2O$ was subtracted from the total free energy of the overall OER reaction, which is equal to 4.92 eV (1.23 × 4), then divided by 4, which gives free energy of OH^-. The free energy for each elementary step at $U = 0$ is calculated and presented in Figure 3e by dotted lines. All OER steps in the free energy diagram at $U = 0$ are uphill meaning endothermic processes. That is at $U = 0$, the OER reaction needs 4.92 eV of energy to proceed, and the equivalent potential (U_{eq}) can be found as 1.23 V (4.92 V/4) since all the four reaction paths should be needed. When equivalent potential is applied (dashed lines in Figure 3e), the formation of O* and OOH* become downhill (i.e., exothermic) for $BaNiO_3$ and $BaNiO_2$, while $BaNi_{0.83}O_{2.5}$ becomes exothermic in formation of O* and OH*.

We defined the overpotential of OER as $\eta_{OER} = U_{OER} - U_{eq}$, where the OER potential (U_{OER}), the least potential necessary for all the reactions to become downhill, was determined by the magnitude of the rate-determining step of OER, $U_{OER} = \max[\Delta G_1, \Delta G_2, \Delta G_3, \Delta G_4]$. In Figure 3e, the overpotential of each perovskite is shown: the $BaNi_{0.83}O_{2.5}$ has the smallest overpotential and $BaNiO_3$ has the largest, which excellently agreed with the outcomes by the calculated e_g-filling. Interestingly, the rate-determining step in all three perovskite oxides is the formation of OO* from HOO*. This indicates that the larger the difference in binding energy of HOO* and OO* intermediates is the better the OER activity. The adsorption energy of OOH decreases (more positive in energy value) in the order of $BaNi_{0.83}O_{2.5}$, $BaNiO_2$, and $BaNiO_3$. The strong binding energy was due to the O in OOH that is bound to the other O. The O in OOH being negatively charged is inclined to the partially positively charged Ba, which stabilizes HOO*. The angle of O−O−Ni in the OOH was measured as 122.34°, 120.61°, and 113.74° for $BaNiO_3$, $BaNiO_2$, and $BaNi_{0.83}O_{2.5}$, and we identified that $BaNi_{0.83}O_{2.5}$ forms a smaller angle than the others. The OO* adsorption energies were determined, and the order of the strength of binding energy was the same as that for the HOO*. This can be explained by the geometry of adsorbed O_2 on the perovskite oxide surfaces. The adsorbing O in OO* on $BaNiO_3$ and $BaNiO_2$ surfaces were bent slightly (about 175° and 142°, respectively). On $BaNi_{0.83}O_{2.5}$, however, both the O adsorbed on Ni, dramatically enhancing the adsorption energy. Although OO* stabilized on $BaNi_{0.83}O_{2.5}$, HOO* also absorbs much more strongly. Therefore, the difference between HOO* and OO* on $BaNi_{0.83}O_{2.5}$ is still larger than the other two. This is the underlying mechanism leading to highest OER activity of $BaNi_{0.83}O_{2.5}$: the difference of the free energies between OO* and HOO* on $BaNi_{0.83}O_{2.5}$ is maximized among the three perovskite oxides as represented by the smallest overpotential. If we can find a perovskite that can still adsorb HOO* strongly but binds OO* more weakly, we can lower overpotential.

CONCLUSIONS

We provided basic information on the interplay between crystal structures of the $BaNiO_3$ and $BaNi_{0.83}O_{2.5}$ and OER activity for the first time. The phase transformation of $BaNiO_3$ into $BaNi_{0.83}O_{2.5}$ appeared during the OER cycling. The OER activity of $BaNi_{0.83}O_{2.5}$ was comparable to those of state-of-the-art BSCF82 and double perovskites. It is associated with the change in e_g occupancy and local structures of Ni between the $BaNiO_3$ and the $BaNi_{0.83}O_{2.5}$. First, e_g occupancy near zero of the $BaNiO_3$ was changed into e_g occupancy near unity of the

DOI: 10.1021/jacs.6b00036
J. Am. Chem. Soc. 2016, 138, 3541−3547

$BaNi_{0.83}O_{2.5}$. Second, the change in Ni local structure was derived from the formation of Ni vacancy in the $BaNiO_3$, and a concomitant decrease ($Ni^{4+} \rightarrow Ni^{2+}/Ni^{3+}$) in the Ni oxidation state (supermixed valence) altered f-s coordination into P coordination. Moreover, the $BaNi_{0.83}O_{2.5}$ showed stable OER activity during 250 cycles because of the O p-band center for Ni neither too close nor too far from the Fermi level. Lastly, the difference between the free energy of OO* and HOO* of $BaNi_{0.83}O_{2.5}$ was the smallest in this study, which leads to achieving the smallest overpotential. All experimental results corresponded to the results calculated by DFT and suggestions previously reported by several authors. Hence, we suggest that $BaNi_{0.83}O_{2.5}$ can be a new family of perovskite catalysts for the OER in alkaline media, and the formation of B-site defects (ABO_3) would be a way to enhance the OER activity of the hexagonal perovskite catalysts.

■ ASSOCIATED CONTENT

Supporting Information

The Supporting Information is available free of charge on the ACS Publications website at DOI: 10.1021/jacs.6b00036.

Experimental details, scanning-electron microscopy (SEM) images, energy-dispersive spectroscopy (EDS) analysis, schematic of $BaNiO_3$ and $BaNiO_2$ crystal structures, potential calibration of reference electrode, nitrogen adsorption−desorption isotherm, cyclic voltammograms for electrochemical surface area (ECSA) calcluations, specific oxygen-evolution reaction (OER) activities normalized by ECSA and BET, high-resolution transmission electron microscopy (HRTEM) images and elemental mapping images, chronopotentiometric responses, X-ray diffranction (XRD) patterns of $BaNiO_3$ catalysts after three OER cycles, and Ni K-edge XANES spectra, Ni L-edge XAS spectra, and O K-edge XAS spectra before and after OER cycles (PDF)

■ AUTHOR INFORMATION

Corresponding Authors

*shulyg@yonsei.ac.kr

*bchan@yonsei.ac.kr

Author Contributions

§J.G.L. and J.H. contributed equally.

Notes

The authors declare no competing financial interest.

■ ACKNOWLEDGMENTS

We acknowledge STEM sample preparation & STEM measurements by H. B. Bae & T. W. Lee at Korea Advanced Institute of Science & Technology analysis centre for research advancement. We thank T. J. Shin et al. for their assistance at the Pohang Light Source (PLS) at beamline 6D and 10D of the Pohang Accelerator Laboratory (PAL). This work was supported by the New and Renewable Energy R&D Program (Grant 20113020030020) under the Ministry of Knowledge Economy, Republic of Korea, the Global Frontier R&D Program (Grant 2013M3A6B1078882) on Global Frontier Hybrid Interface Materials R&D Center of the National Research Foundation of Korea (NRF) funded by the Ministry of Science, ICT and Future Planning, and the New & Renewable Energy Core Technology Program of the Korea Institute of Energy Technology Evaluation and Planning (KETEP) granted financial resource from the Ministry of Trade, Industry & Energy, Republic of Korea (Grant No. 20133030011320).

■ REFERENCES

(1) Tarascon, J.-M.; Armand, M. *Nature* **2001**, *414*, 359.
(2) McCrory, C. C. L.; Jung, S.; Peters, J. C.; Jaramillo, T. F. *J. Am. Chem. Soc.* **2013**, *135*, 16977.
(3) Kanan, M. W.; Nocera, D. G. *Science* **2008**, *321*, 1072.
(4) Koper, M. T. M. *J. Electroanal. Chem.* **2011**, *660*, 254.
(5) Suntivich, J.; May, K. J.; Gasteiger, H. A.; Goodenough, J. B.; Shao-Horn, Y. *Science* **2011**, *334*, 1383.
(6) Yagi, S.; Yamada, I.; Tsukasaki, H.; Seno, A.; Murakami, M.; Fujii, H.; Chen, H.; Umezawa, N.; Abe, H.; Nishiyama, N.; Mori, S. *Nat. Commun.* **2015**, *6*, 8249.
(7) Chen, C. − F.; King, G.; Dickerson, R. M.; Papin, P. A.; Gupta, S.; Kellogg, W. R.; Wu, G. *Nano Energy* **2015**, *13*, 423.
(8) Risch, M.; Grimaud, A.; May, K. J.; Stoerzinger, K. A.; Chen, T. J.; Mansour, A. N.; Shao-Horn, Y. *J. Phys. Chem. C* **2013**, *117*, 8628.
(9) Bockris, J. O. M.; Otagawa, T. *J. Electrochem. Soc.* **1984**, *131*, 290.
(10) May, K. J.; Carlton, C. E.; Stoezinger, K. A.; Risch, M.; Suntivich, J.; Lee, Y.-L.; Grimaud, A.; Shao-Horn, Y. *J. Phys. Chem. Lett.* **2012**, *3*, 3264.
(11) Carbonio, R. E.; Fierro, C.; Tryk, D.; Scherson, D.; Yeager, E. *J. Power Sources* **1988**, *22*, 387.
(12) Grimaud, A.; May, K. J.; Carlton, C. E.; Lee, Y.-L.; Risch, M.; Hong, W. T.; Zhou, J.; Shao-Horn, Y. *Nat. Commun.* **2013**, *4*, 2439.
(13) Grimaud, A.; Carlton, C. E.; Risch, M.; Hong, W. T.; May, K. J.; Shao-Horn, Y. *J. Phys. Chem. C* **2013**, *117*, 25926.
(14) Shibahara, H. *J. Solid State Chem.* **1987**, *69*, 81.
(15) Gottschall, R.; Schollhorn, R.; Muhler, M.; Jansen, N.; Walcher, D.; Gutlich, P. *Inorg. Chem.* **1998**, *37*, 1513.
(16) Campa, J. A.; Gutierrez-Puebla, E.; Monge, M. A.; Rasines, I.; Ruiz-Valero, C. *J. Solid State Chem.* **1994**, *108*, 230.
(17) Rossmeisl, J.; Qu, Z.-W.; Zhu, H.; Kroes, G.-J.; Nørskov, J. K. *J. Electroanal. Chem.* **2007**, *607*, 83.
(18) Doyle, R. L.; Lyons, M. E. G. *Phys. Chem. Chem. Phys.* **2013**, *15*, 5224.
(19) Man, I. C.; Su, H. − Y.; Calle-Vallejo, F.; Hansen, H. A.; Martínez, J. I.; Inoglu, N. G.; Kitchin, J.; Jaramillo, T. F.; Nørskov, J. K.; Rossmeisl, J. *ChemCatChem* **2011**, *3*, 1159.
(20) Boltersdorf, J.; King, N.; Maggard, P. A. *CrystEngComm* **2015**, *17*, 2225.
(21) Lyons, M. E. G.; Brandon, M. P. *Int. J. Electrochem. Sci.* **2008**, *3*, 1386.
(22) Kim, M.-S.; Kim, K.-B. *J. Electrochem. Soc.* **1998**, *145*, 507.
(23) Klaus, S.; Cai, Y.; Louie, M. W.; Trotochaud, L.; Bell, A. T. *J. Phys. Chem. C* **2015**, *119*, 7243.
(24) Subbaraman, R.; Tripkovic, D.; Chang, K. − C.; Strmcnik, D.; Paulikas, A. P.; Hirunsit, P.; Chan, M.; Greeley, J.; Stamenkovic, V.; Markovic, N. M. *Nat. Mater.* **2012**, *11*, 550.
(25) Chen, D.; Chen, C.; Baiyee, Z. M.; Shao, Z.; Ciucci, F. *Chem. Rev.* **2015**, *115*, 9869.
(26) Qiu, Y.; Xin, L.; Li, W. *Langmuir* **2014**, *30*, 7893.
(27) Zhu, Y.; Zhou, W.; Chen, Z. − G.; Chen, Y.; Su, C.; Tade, M. O.; Shao, Z. *Angew. Chem., Int. Ed.* **2015**, *54*, 3897.
(28) Zhu, Y.; Zhou, W.; Chen, Y.; Yu, J.; Liu, M.; Shao, Z. *Adv. Mater.* **2015**, *27*, 7150.
(29) Liu, R.; Liang, F.; Zhou, W.; Yang, Y.; Zhu, Z. *Nano Energy* **2015**, *12*, 115.
(30) Zhou, W.; Zhao, M.; Liang, F.; Smith, S. C.; Zhu, Z. *Mater. Horiz.* **2015**, *2*, 495.
(31) McCrory, C. C. L.; Jung, S.; Ferrer, I. M.; Chatman, S. M.; Peters, J. C.; Jaramillo, T. F. *J. Am. Chem. Soc.* **2015**, *137*, 4347.
(32) Hammer, B.; Norskov, J. K. *Nature* **1995**, *376*, 238.
(33) Hong, W. T.; Risch, M.; Stoerzinger, K. A.; Grimaud, A.; Suntivich, J.; Shao-Horn, Y. *Energy Environ. Sci.* **2015**, *8*, 1404.
(34) Mefford, J. T.; Hardin, W. G.; Dai, S.; Johnston, K. P.; Stevenson, K. J. *Nat. Mater.* **2014**, *13*, 726.

DOI: 10.1021/jacs.6b00036
J. Am. Chem. Soc. 2016, 138, 3541−3547

(35) Gong, M.; Zhou, W.; Tsai, M. − C.; Zhou, J.; Guan, M.; Lin, M. − C.; Zhang, B.; Hu, Y.; Wang, D. − Y.; Yang, J.; Pennycook, S. J.; Hwang, B. − J.; Dai, H. *Nat. Commun.* **2014**, *5*, 4695.
(36) Mansour, A. N.; Melendres, C. A.; Pankuch, M.; Brizzolara, R. A. *J. Electrochem. Soc.* **1994**, *141*, L69.
(37) Gu, W.; Wang, H.; Wang, K. *Dalton Trans.* **2014**, *43*, 6406.
(38) Soriano, L.; Gutiérrez, A.; Preda, I.; Palacín, S.; Sanz, J. M.; Abbate, M.; Trigo, J. F.; Vollmer, A.; Bressler, P. R. *Phys. Rev. B: Condens. Matter Mater. Phys.* **2006**, *74*, 193402.
(39) Rossmeisl, J.; Logadottir, A.; Norskov, J. K. *Chem. Phys.* **2005**, *319*, 178.
(40) Han, B. C.; Viswanathan, V.; Pitsch, H. *J. Phys. Chem. C* **2012**, *116*, 6174.
(41) Goodenough, J. B.; Manoharan, R.; Paranthaman, M. *J. Am. Chem. Soc.* **1990**, *112*, 2076.
(42) Nørskov, J. K.; Rossmeisl, J.; Logadottir, A.; Lindqvist, L.; Kitchin, J. R.; Bligaard, T.; Jónsson, H. *J. Phys. Chem. B* **2004**, *108*, 17886.

DOI: 10.1021/jacs.6b00036
J. Am. Chem. Soc. 2016, 138, 3541−3547